Article

Pseudospin-polarized slow light waveguides with large delay-bandwidth product

Check for updates

Fu-Long Shi, Xiao-Dong Chen [ORCID], Wen-Jie Chen [ORCID] ✉ & Jian-Wen Dong [ORCID] ✉

Delay-bandwidth product (DBP) is a key metric in slow light waveguides, requiring a balance between a large group index and broad bandwidth—two parameters that often involve a trade-off. Here, we propose and demonstrate a slow light waveguide with large DBP using a pseudospin-polarized transverse electromagnetic mode. This waveguide features a folded edge configuration that supports a 200% relative bandwidth from quasistatic limit (zero frequency) and an arbitrarily large group index. Owing to the pseudospin-polarized design, the dense folding would not introduce backscattering and the associated group velocity dispersion (GVD). The resulting gapless linear dispersion and pulse transmission behavior in folded edge waveguide are observed in microwave experiments. Our scheme provides a way to overcome the trade-off between group index and working bandwidth in slow light waveguide, which has potential applications in broadband optical buffering, light-matter interaction enhancement, terahertz radiation source and time domain processing.

Slow light refers to the reduction of the group velocity of light, which facilitates time-domain processing of optical signals[1] and has promising applications in optical buffering[2,3], light-matter interaction enhancement[4,5], terahertz radiation source[6], switching[7,8], etc. This effect can generally be achieved through extremely strong dispersion either in bulk materials (electromagnetically induced transparency[7,9–11], coherent population oscillations[12,13], stimulated Brillouin scattering[14,15], stimulated Raman scattering[16], etc) or in artificially engineered structures (photonic crystals[17–24], coupled resonators[2,25], gratings[26,27], etc). The latter approach has been intensively studied due to its compatibility with on-chip integration.

A fundamental challenge in slow-light systems is the trade-off between relative working bandwidth ($\Delta f/f_m$, where Δf is the working bandwidth and f_m is the center frequency) and group index (n_g), which is indicated by delay-bandwidth product $DBP = n_g \left(\frac{\Delta f}{f_m}\right)$[26,28,29]. For instance, in typical photonic-wire waveguides in Fig. 1a, reducing group velocity is typically accompanied by a narrowing of the working bandwidth, due to the limited momentum range occupied by the slow-light band. Thus, slow light is only achievable in a finite frequency range[30] [depicted in the blue shaded area of Fig. 1b]. Relative bandwidth of the photonic-wire waveguide is usually <10% and group index is usually <10, resulting in a DBP < 1. A similar trade-off is observed in photonic crystal (PC) line defect waveguide. In a PC line defect waveguide indicated in Fig. 1c, slow light can be achieved near the Brillouin zone boundary of dispersion [blue shaded area in Fig. 1d] due to the crossing

coupling between forward and backward guided modes[29]. Relative bandwidth of the PC line defect waveguide is typically <10%, with a group index <100, yielding a DBP < 10. DBP in both photonic-wire waveguide and PC line defect waveguide are restricted by the momentum range occupied by the slow-light band. Recently, an alternative scheme was proposed to generate a slow-light band winding along the Brillouin zone multiple times by carefully engineering the edge structure or adding side-coupled resonators, utilizing the gapless edge mode of topological photonic crystals[31–33]. Although the proposed scheme relaxes the fundamental limitation in momentum space, the DBP of the slow-light device is still limited by the narrow frequency bandwidth due to the crystal's multiple scattering mechanism and the weak magneto-optical effect of natural materials. Furthermore, the nonlinearity of dispersion in these designs introduces group velocity dispersion (GVD), leading to signal deformation. To address these challenges, it is desirable to relax both bandwidth and momentum space limitations in a time-reversal invariant manner, ideally without relying on external magnetic fields. Additionally, minimizing GVD is crucial for maintaining signal integrity in slow-light systems.

In this article, we propose a slow light waveguide with working frequency spanning from quasistatic limit (zero frequency) to a finite frequency, corresponding to the maximal relative bandwidth of 200%, and demonstrate a large DBP of 40. Here we use a simple metallic structure to realize a slow light waveguide without applying external field. By periodically folding the metal edge in real space, its gapless linear dispersion of

School of Physics & State Key Laboratory of Optoelectronic Materials and Technologies, Sun Yat-sen University, Guangzhou, 510275, China.
✉e-mail: chenwenj5@mail.sysu.edu.cn; dongjwen@mail.sysu.edu.cn

1

Fig. 1 | Comparison of the pseudospin-polarized slow light waveguide and other two types of slow light waveguides. a Schematic of a photonic-wire waveguide. **b** Dispersion and group index of photonic-wire waveguide. In this type of waveguides, slow light can be obtained in a finite frequency regime (shaded in blue), relative bandwidth is usually <10% and group index is usually <10. **c** Schematic of a photonic crystal (PC) line defect waveguide. **d** Dispersion and group index of PC line defect waveguide. In PC line defect waveguides, slow light can be achieved near the Brillouin zone boundary (middle in the figure) due to the crossing coupling between forward and backward guided modes. Its relative bandwidth is usually <10% and group index is usually <100. **e** Schematic of a pseudospin-polarized folded edge waveguide. **f** Dispersion and group index of folded edge waveguide. In this type of waveguides, pseudospin-polarized edge mode (blue lines) exists from zero frequency to a finite frequency, naturally indicating a relative bandwidth of 200%. Group index can be increased by lengthening the optical path via a folded edge configuration. Thus, an extremely large DBP can be obtained. This densely folding would not introduce backscattering and subsequent GVD, due to pseudospin-momentum locking.
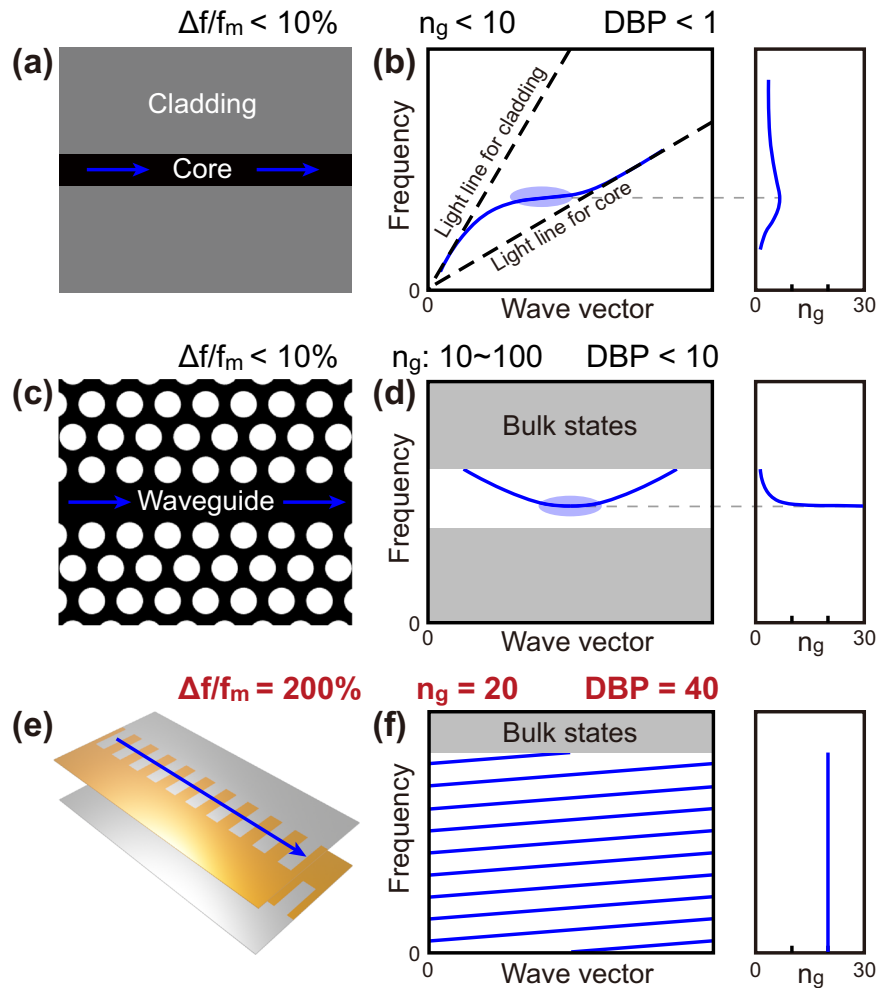
pseudospin-polarized edge modes in momentum space would wind around the Brillouin zone multiple times and cover the frequency region starting from zero frequency, leading to a theoretically unlimited DBP and a negligible GVD. The linear dispersion of slow light waveguide was experimentally verified through field-mapping measurement. Pulse transmission along the folded edge waveguide was also demonstrated. The experimental results demonstrate the capability of constructing a slow light waveguide utilizing the pseudospin-polarized folded edge channel. Moreover, the signal transport in the folded edge waveguide is robust against backscattering for its pseudospin-momentum locked feature, while signal transport in conventional slow light system is usually vulnerable to backscattering for the enhanced light-matter interaction.

Results

Design of pseudospin-polarized slow light waveguide

Backscattering-immune edge states traversing bulk gap are a feature of topological insulators and the analogs in classical wave systems[34–46]. One example is the quantum spin Hall insulator, where the pseudospin of the edge state is locked to its linear momentum[47,48]. Further research found that such pseudospin-polarized states are not exclusive to the edges of topological systems. They can also be realized in channels with boundaries supporting certain dual symmetries[49]. One of the simplest implementations of this concept is a pseudospin-polarized edge formed between two PEC-PMC (perfect electric conductor - perfect magnetic conductor) parallel plate waveguides. This design enables the backscattering-immune transport of electromagnetic signal along arbitrary paths over a very broad frequency range.

Utilizing the pseudospin-polarized edge mode, a straightforward method to slow down electromagnetic waves is to construct a periodically folded edge waveguide [Fig. 1e], which naturally increases the optical path length and enhances the effective group index. Dispersion and group index of the folded edge waveguide are plotted in Fig. 1f. The relative bandwidth is 200%, as the pseudospin-polarized edge mode extends from zero frequency. Additionally, the group index of the folded edge waveguide is comparable to that of PC line defect waveguide, reaching values of 20 or higher. Consequently, an extremely large DBP of 40 or greater can be achieved. Note that the folding of the edge waveguide, regardless of the sharpness of the corners, does not induce backscattering and the resultant band gap opening at Brillouin zone boundary[49]. This is the fundamental difference between conventional folded waveguide and our design.

The design begins with a perfect electrical conductor (PEC) edge waveguide supporting pseudospin-polarized edge modes as shown in Fig. 2a. This can be considered equivalent to the pseudospin-polarized PEC-PMC edge waveguide (more discussion can be seen in Supplementary Note 1). The edge (blue solid line) is formed between two stacks of PEC plates with a spacing of $h = a$, where $a = 20$ mm is defined as a unit length. Each stack functions as a series of PEC parallel plate waveguides, where transverse electric mode cannot propagate but evanescently decay below a cutoff frequency of $f_c = \frac{c}{2h} = 7.5$ GHz. However, when two stacks of PEC plates with an offset of $h/2$ are put together, two counter-propagating edge modes strongly confined near the edge would emerge. These two edge modes are both transverse electromagnetic modes (TEM modes)[49,50] and exhibit linear dispersion of $\omega = 2\pi f = c|k_x|$ with the speed of light c, see Fig. 2b. Figure 2c shows the eigen electric field (magenta arrows) and
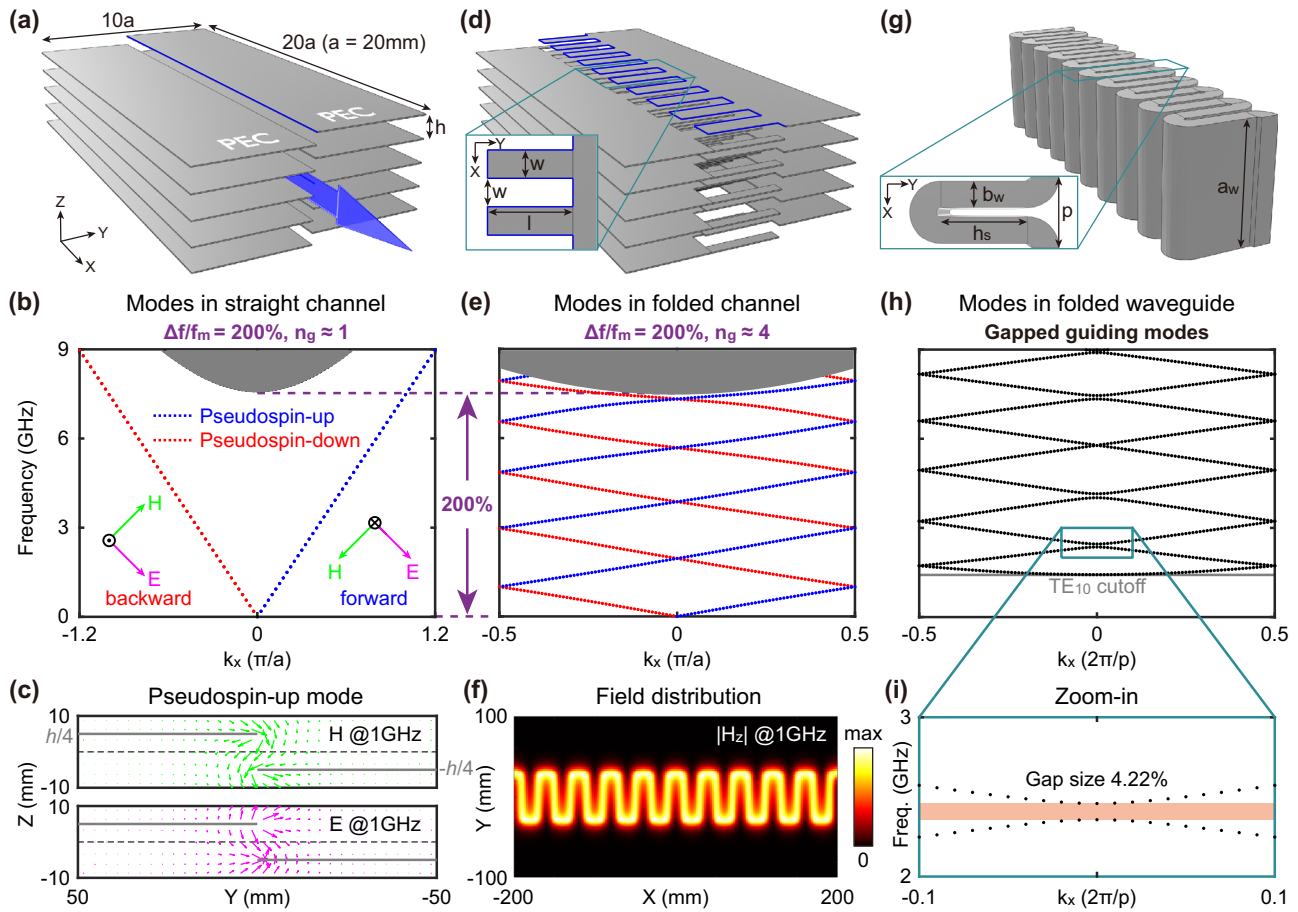
Fig. 2 | Pseudospin-polarized slow light waveguide by constructing a backscattering-immune folded edge channel. a Pseudospin-polarized edge waveguide composed of two stacks of metallic plates that can be seen as perfect electrical conductor (PEC). Transverse electromagnetic (TEM) modes are guided along the straight edge (blue line) between two stacks. **b** Dispersion relation of the pseudospin-polarized edge mode. Two edge bands (blue and red dotted lines) exist from zero frequency for their TEM feature. The insets show the electric and magnetic vector of the forward-propagating pseudospin-up edge mode (corresponding to blue dotted line) and the backward-propagating pseudospin-down edge mode (corresponding to red dotted line). **c** Eigen EM fields of the pseudospin-up edge mode at 1 GHz. **d** Pseudospin-polarized waveguide with a folded edge. The inset shows the groove structure in the top layer. The groove structures of two sets of metallic plates are complementary to each other to preserve the effective dual symmetry. **e** Gapless dispersion for the folded edge waveguide. The pseudospin-polarized bands remain linear and gapless below the cutoff frequency, implying that the folding introduce a group delay but no backscattering. **f** H_z amplitude profile of the EM wave propagating along the folded edge. **g** Conventional folded waveguide by folding a rectangular metallic waveguide. The inset shows the top-view of one unit. **h** Gapped dispersion for the folded rectangular waveguide. Note that band gaps open at Brillouin zone center for the sake of backscattering occurred at waveguide bends. These quadratic dispersions near band gaps would lead to nonzero GVD and limit the working bandwidth. **i** Zoom-in of the gapped dispersion around 2.5 GHz.

magnetic field (green arrows) of the forward-propagating pseudospin-up edge mode. The electric and magnetic field distributions of the forward-propagating edge mode within $z \in (-h/4, h/4)$ form an anti-mirror reflection about the xy plane (black dashed line), due to an effective dual symmetry[49]. Conversely, the electric and magnetic fields of the backward-propagating edge mode form a mirror reflection about the xy plane [show in inset of Fig. 2b]. These anti-symmetric and symmetric modes belong to different subspaces of the system and thus are decoupled from each other, as long as translational symmetry in z-direction and mirror symmetry are preserved[49]. These antisymmetric (symmetric) modes are termed as pseudospin-up (pseudospin-down) polarized modes, highlighted in blue (red) in Fig. 2b. Hence this edge waveguide exhibits pseudospin-momentum locking and supports backscattering-immune transport. Note that such PEC waveguide also supports additional waveguide modes [not shown in Fig. 2b], such as E_z-polarized plane wave modes. However, these additional modes are decoupled from the pseudospin-polarized edge modes due to their different parities and can be selectively excited (see more discussions in Supplementary Note 2).

To increase time delay and to slow down the group velocity, the straight edge can be bent into a folded edge with a groove shape, where the groove

depth $l = 3a$, groove width $w = a$ and period $2w$, as illustrated in Fig. 2d. The groove width w must be more than twice the transverse decay length of edge mode 8.52 mm (see Supplementary Note 4 and 6 for more details on the decay length). To maintain system symmetry and decoupling of pseudospins, two complementary sets of PEC plates are alternately stacked along the z-axis. Since the pseudospin-polarized edge mode can pass through each corner without reflection [Fig. 2f], the time delay introduced by corners is minimal. The group index of the folded edge is approximately proportional to the total length per propagation period. Figure 2e shows the band dispersion of the folded edge waveguide. Although the bands are folded between Brillouin zone boundaries due to the introduction of periodicity, the pseudospin-polarized nature of the modes is preserved. The average group index can be calculated from the slope of edge band, averaged from zero to the cutoff frequency: $\bar{n}_g = c \cdot \frac{k_t}{\omega_t} = 4.25$ ($\bar{n}_g$ is average group index, c is speed of light, k_t is total momentum range of the edge band, ω_t is angular frequency range of the edge band below cutoff frequency $2\pi*7.5$ GHz). It is noteworthy that the band folding does not introduce any gap opening, confirming the decoupling of pseudospins. As a result, the edge mode remains gapless and linear from zero to a finite frequency, corresponding to a 200% relative bandwidth. The linearity indicates a very small GVD, which
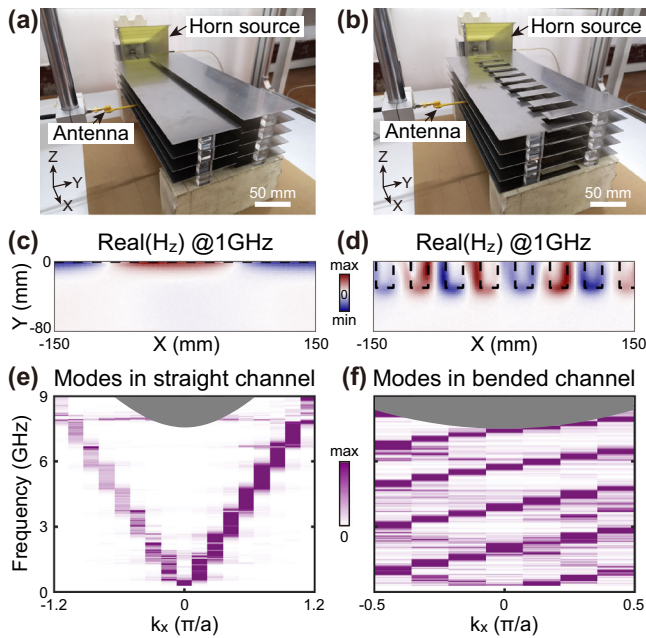
Fig. 3 | Measured dispersions of straight/folded edge waveguides.
a, b Experimental setups for scanning the EM fields inside the straight/folded edge waveguides. Experimental structures correspond to the simulated structures in Fig. 2a, d. Scale bars represent 50 mm. **c, d** Measured H_z fields at 1 GHz. It shows that EM waves are well confined and guided along the edges (black dashed lines). **e, f** Edge dispersions obtained by Fourier transforming the scanned H_z fields. Weak signals corresponding to pseudospin-down backward modes appear due to reflection at the output ends of waveguides.
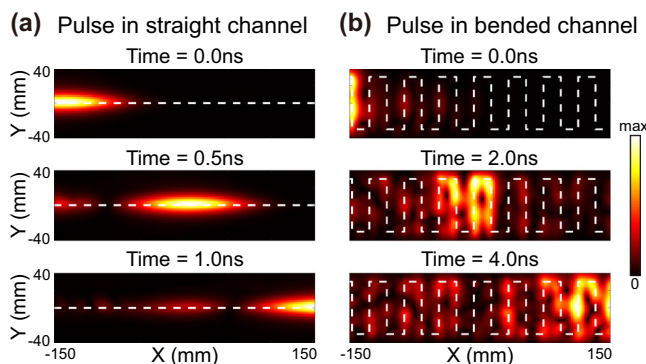
Fig. 4 | Pulse transmission in the straight/folded edge waveguide. a Snapshots of measured amplitude profiles at Time = 0.0 ns, 0.5 ns and 1.0 ns for the straight edge. The input Gaussian pulse is centered at 4 GHz and has a full bandwidth at half maximum of 3 GHz. **b** Snapshots of measured amplitude profiles at Time = 0.0 ns, 2.0 ns and 4.0 ns for the folded edge. Pulse transmission time in folded edge waveguide is 4.4 times of that in straight edge waveguide, indicating that the group index is increased from 1 to about 4.

is another concerned issue in slow light device. Collectively, these features make this system an ideal platform for broadband slow light device with very low GVD.

For comparison, we also simulate a conventional folded waveguide based on rectangular waveguide (broad wall dimension $a_w = 105$ mm, narrow wall dimension $b_w = 15$ mm, straight height $h_s = 48.6$ mm, period of pitch $p = 40$ mm), as shown in Fig. 2g. Its working frequency begins at a nonzero value of 1.43 GHz, corresponding to the cutoff frequency of TE_{10} mode, rather than the quasistatic limit. In Fig. 2h, multiple band gaps of TE_{10} modes are observed at the Brillouin zone center, resulting from scattering between forward and backward modes, which creates a gapped dispersion.

Specifically, a 4.22% gap around 2.5 GHz open as shown in Fig. 2i. These gaps naturally restrict the working bandwidth of the folded waveguide. Additionally, the quadratic dispersions near band edges would inevitably result in significant GVD, which is undesirable for signal transport.

Microwave measurement of slow light transport

To demonstrate our concept in microwave regime, we fabricated two samples of edge waveguides: one with straight edge [Fig. 3a] and the other with folded edge [Fig. 3b]. The geometry of both edge waveguides matches those shown in Fig. 2a, d. Each sample consist of two sets of complementary steel plates stacked in z-direction (5 periods). Two representative H_z field patterns measured at 1 GHz are plotted in Fig. 3c, d, for the straight edge and the folded edge (see field patterns at more frequencies in Supplementary Note 3). Due to measurement limitations, only the lower half of each field pattern is shown. The measured electromagnetic fields are strongly confined and guided along both edges (black dashed lines). By summarizing the Fourier spectra of scanned H_z fields across various frequencies, the band dispersions of pseudospin-polarized edge modes are mapped in Fig. 3e, f. As expected, edge folding does not introduce any minigap at Brillouin zone boundaries. The gapless dispersion of pseudospin-up (pseudospin-down) edge mode winds along Brillouin zone multiple times, resulting in a broadband slow light effect starting from zero frequency. Although the folded edge sample in our experiment achieved a group index of only about 4, this could in principle be increased by simply extending the perimeter of folded edge. In addition, Fourier components of the forward band are apparently stronger than that of the backward mode due to the excitation from the source horns. Weaker signals for backward edge band are attributed to the small reflectance at waveguide exit.

A more direct method to verify broadband slow light effect is to conduct a pulse transmission experiment. In this experiment, a Gaussian pulse was loaded onto the measured signal in the frequency domain, and the time-domain pulse transmission results were obtained by performing Fourier transform (see Methods). The pulse had a center frequency of 4 GHz and a full bandwidth at half maximum (FBHM) of 3 GHz, with its envelope nearly covering the working frequency range of 0 to 7.5 GHz. Figure 4a, b shows the snapshots of intensity profiles at various time intervals over a 300 mm-long section around the edge waveguides. The moment the pulse center reaches the left end of the measured area is defined as time zero. The pulse transmission times for the straight and folded edge waveguides were 1.0 ns and 4.4 ns, respectively. Since the pseudospin mode guided along a straight edge waveguide is a TEM mode, its group velocity is expected to be c (the speed of light in vacuum). Thus the group index of folded edge waveguide can be estimated by the ratio of the transmission times 4.4 ns (folded) and 1.0 ns (straight), that is equal to 4.4. The pulse transmission results further demonstrate the slow light effect with a group index close to 4.25.

Achieve a large delay-bandwidth product

Although a folded edge waveguide with the group index of 4.4 is demonstrated in our experiment, a waveguide with an arbitrary large group index n_g can theoretically be achieved, which would be numerically confirmed below. The group index is approximately the ratio of the edge path length per propagation period, $(l + w) / w$, and can be increased by either enlarging groove depth l or reducing groove width w (a fractal edge waveguide for achieving a large group index is also presented in Supplementary Note 5). The calculated group index n_g in Fig. 5a shows good agreement with the path length ratio $(l + w) / w$. As an example, Fig. 5b shows the edge mode dispersion for the case where $l = 19a$, $w = a$ and $h = a$ [red diamond in Fig. 5a]. The average group index in this case is $n_g = 20.26$. From blue curve in Fig. 5c, it is found that the group index fluctuates around 20. This fluctuation is due to side couplings between adjacent edges caused by the narrow width w, which is evidenced by the wandering path of light in Fig. 5d. Such couplings could result in undesired GVD near these frequencies. One approach to address this issue is to minimize the transverse decay length of the edge mode by reducing the vertical spacing h. As shown in Fig. 5e, the transverse decay length is proportional to h due to the scaling property of
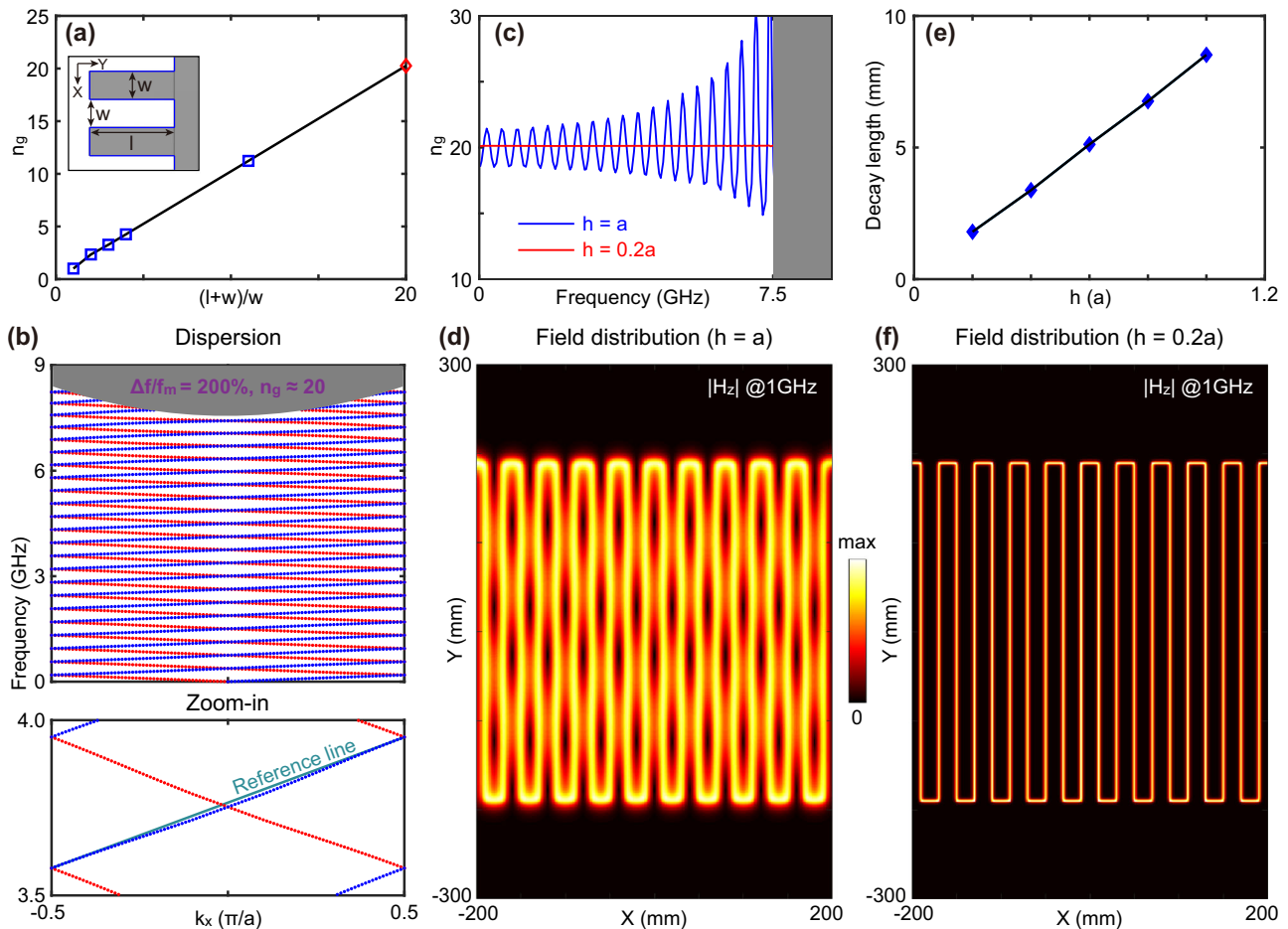
Fig. 5 | Large DBP by lengthening the optical path of folded edge. a Group index as a function of the path length ratio $(l + w) / w$. The inset shows the groove structure of the folded edge and the geometry parameters. **b** Dispersion of the edge states of the waveguide with $l = 19a$, $w = a$ and $h = a$. DBP of the folded edge waveguide is approximately 40. Zoom-in of the dispersion within 3.5–4.0 GHz is plotted, and a reference straight line is added to show the slight nonlinear of the dispersion. **c** Group index for different values of h. Fluctuations in group index are caused by the side coupling between adjacent edges and the resultant slight nonlinear of edge dispersion, see the zoom-in plot in **b**. Red curve shows the group index for $h = 0.2a$, showing a nearly constant group index of 20. Further lowering h would lead to more localized EM field and less side coupling between adjacent edges. **d** Field profile for the case of $h = a$. **e** Transverse decay lengths of the H_z fields for different h. **f** Field profile for the case of $h = 0.2a$.

Maxwell's equations (see Supplementary Note 4 for details). By decreasing the spacing to $h = 0.2a$, side couplings between adjacent edges becomes negligible [as illustrated in the field pattern in Fig. 5f]. Consequently, the group index becomes almost constant [red curve in Fig. 5c], indicating that the edge dispersion becomes more linear with reduced GVD. Thus, a slow light waveguide with an extremely large DBP of $20.26 \times 200\% = 40.52$ is numerically demonstrated.

Conclusions

In conclusion, we have proposed and demonstrated a pseudospin-polarized slow light waveguide. Due to its pseudospin-polarized properties, electromagnetic wave can be confined within a densely folded channel without introducing backscattering. This enables a linear dispersion starting from zero frequency, resulting in an extremely large DBP and negligible GVD, both critical parameters for slow light devices. Our scheme relieves the inherent trade-off between a large group index and a wide working bandwidth, which is a fundamental limit on achieving large DBP in slow light application. The multiply folded band dispersion and the pulse transmission process in folded edge waveguide are experimentally observed in microwave regime. This design can be readily extended to the terahertz regime and holds potential for various applications, including broadband optical buffers and terahertz radiation sources.

Methods

Experimental setup

The two samples of edge waveguides are composed of two sets of complementary steel plates stacked in z-direction (5 periods). The steel plates in each stack are separated by air and supported by acrylic blocks positioned at the edge of the sample. An E_y-polarized horn is put 2 cm away from the waveguide entrance to excite the pseudospin-up edge mode propagating along +x direction. A magnetic loop antenna fixed on a motor scanning platform is inserted into the edge area to scan H_z fields inside the sample.

Method of reconstructing pulse transmission results

Time domain pulse transmission images in Fig. 4 is reconstructed based on the microwave near-field measurement. In H_z field pattern measurements, frequency spectrum at the spatial points around the two edge waveguides have been measured. Then the measured frequency signals are reshaped by loading a Gaussian pulse, whose center frequency is 4 GHz and full bandwidth at half maximum (FBHW) is 3 GHz. Time domain pulse signals at each spatial points can be reconstructed by performing an inverse Fourier transform on the reshaped frequency signals. Finally, the snapshots of intensity profiles at different instants can be obtained by collecting time domain signals of all spatial points.

Data availability

The simulated and experimental data supporting the findings of this study are available from the corresponding authors on reasonable request.

References

1. Ginsberg, N. S., Garner, S. R. & Hau, L. V. Coherent control of optical information with matter wave dynamics. *Nature* **445**, 623 (2007).
2. Xia, F., Sekaric, L. & Vlasov, Y. Ultracompact optical buffers on a silicon chip. *Nat. Photonics* **1**, 65–71 (2007).
3. Dahan, D. & Eisenstein, G. Tunable all optical delay via slow and fast light propagation in a Raman assisted fiber optical parametric amplifier: a route to all optical buffering. *Opt. Express* **13**, 6234–6249 (2005).
4. Corcoran, B. et al. Green light emission in silicon through slow-light enhanced third-harmonic generation in photonic-crystal waveguides. *Nat. Photonics* **3**, 206–210 (2009).
5. Kang, H. S., Hernandez, G. & Zhu, Y. F. Slow-light six-wave mixing at low light intensities. *Phys. Rev. Lett.* **93**, 073601 (2004).
6. Gao, L., Hu, Y., Hu, Q., Zhu, X. & Li, B. Study of double-beam folded waveguide back wave oscillator in Terahertz Band. *2018 IEEE International Vacuum Electronics Conference (IVEC),* 401–402 (2018).
7. Zhou, X. et al. Slowing, advancing and switching of microwave signals using circuit nanoelectromechanics. *Nat. Phys.* **9**, 179–184 (2013).
8. Bajcsy, M. et al. Efficient all-optical switching using slow light within a hollow fiber. *Phys. Rev. Lett.* **102**, 203902 (2009).
9. Hau, L. V., Harris, S. E., Dutton, Z. & Behroozi, C. H. Light speed reduction to17metrespersecond in an ultracold atomicgas. *Nature* **397**, 594–598 (1999).
10. Safavi-Naeini, A. H. et al. Electromagnetically induced transparency and slow light with optomechanics. *Nature* **472**, 69–73 (2011).
11. Karpa, L. & Weitz, M. A Stern-Gerlach experiment for slow light. *Nat. Phys.* **2**, 332–335 (2006).
12. Bigelow, M. S., Lepeshkin, N. N. & Boyd, R. W. Superluminal and slow light propagation in a room-temperature solid. *Science* **301**, 200–202 (2003).
13. Ku, P.-C. et al. Slow light in semiconductor quantum wells. *Opt. Lett.* **29**, 2291 (2004).
14. Kim, J., Kuzyk, M. C., Han, K. W., Wang, H. L. & Bahl, G. Non-reciprocal Brillouin scattering induced transparency. *Nat. Phys.* **11**, 275–280 (2015).
15. Okawachi, Y. et al. Tunable all-optical delays via Brillouin slow light in an optical fiber. *Phys. Rev. Lett.* **94**, 153902 (2005).
16. Sharping, J. E., Okawachi, Y. & Gaeta, A. L. Wide bandwidth slow light using a Raman fiber amplifier. *Opt. Express* **13**, 6092 (2005).
17. Vlasov, Y. A., O'Boyle, M., Hamann, H. F. & McNab, S. J. Active control of slow light on a chip with photonic crystal waveguides. *Nature* **438**, 65–69 (2005).
18. Ek, S. et al. Slow-light-enhanced gain in active photonic crystal waveguides. *Nat. Commun.* **5**, 5039 (2014).
19. Li, J., White, T. P., O'Faolain, L., Gomez-Iglesias, A. & Krauss, T. F. Systematic design of flat band slow light in photonic crystal waveguides. *Opt. Express* **16**, 6227 (2008).
20. Mori, D. & Baba, T. Wideband and low dispersion slow light by chirped photonic crystal coupled waveguide. *Opt. Express* **13**, 9398–9408 (2005).
21. Castellanos Munoz, M. et al. Optically induced indirect photonic transitions in a slow light photonic crystal waveguide. *Phys. Rev. Lett.* **112**, 053904 (2014).
22. Arregui, G., Gomis-Bresco, J., Sotomayor-Torres, C. M. & Garcia, P. D. Quantifying the robustness of topological slow light. *Phys. Rev. Lett.* **126**, 027403 (2021).
23. Chen, J., Liang, W. & Li, Z.-Y. Switchable slow light rainbow trapping and releasing in strongly coupling topological photonic systems. *Photonics Res.* **7**, 1075–1080 (2019).
24. Chen, J., Liang, W. & Li, Z. Y. Broadband dispersionless topological slow light. *Opt. Lett.* **45**, 4964–4967 (2020).
25. Yanik, M. F. & Fan, S. Stopping light all optically. *Phys. Rev. Lett.* **92**, 083901 (2004).
26. Mok, J. T., de Sterke, C. M., Littler, I. C. M. & Eggleton, B. J. Dispersionless slow light using gap solitons. *Nat. Phys.* **2**, 775–780 (2006).
27. Gan, Q., Fu, Z., Ding, Y. J. & Bartoli, F. J. Ultrawide-bandwidth slow-light system based on THz plasmonic graded metallic grating structures. *Phys. Rev. Lett.* **100**, 256803 (2008).
28. Xu, Q. F., Dong, P. & Lipson, M. Breaking the delay-bandwidth limit in a photonic structure. *Nat. Phys.* **3**, 406–410 (2007).
29. BaBa, T. Slow light in photonic crystals. *Nat. Phontonics* **2**, 465 (2008).
30. Dulkeith, E., Xia, F., Schares, L., Green, W. M. J. & Vlasov, Y. A. Group index and group velocity dispersion in silicon-on-insulator photonic wires. *Opt. Express* **14**, 3853 (2006).
31. Guglielmon, J. & Rechtsman, M. C. Broadband topological slow light through higher momentum-space winding. *Phys. Rev. Lett.* **122**, 153904 (2019).
32. Mann, S. A. & Alù, A. Broadband topological slow light through Brillouin zone winding. *Phys. Rev. Lett.* **127**, 123601 (2021).
33. Chen, F. et al. Multiple Brillouin zone winding of topological chiral edge states for slow light applications. *Phys. Rev. Lett.* **132**, 156602 (2024).
34. Wang, Z., Chong, Y., Joannopoulos, J. & Soljačić, M. Reflection-free one-way edge modes in a gyromagnetic photonic crystal. *Phys. Rev. Lett.* **100**, 013905 (2008).
35. Wang, Z., Chong, Y., Joannopoulos, J. D. & Soljačić, M. Observation of unidirectional backscattering-immune topological electromagnetic states. *Nature* **461**, 772–775 (2009).
36. Poo, Y., Wu, R.-X., Lin, Z., Yang, Y. & Chan, C. T. Experimental realization of self-guiding unidirectional electromagnetic edge states. *Phys. Rev. Lett.* **106**, 093903 (2011).
37. Khanikaev, A. B. et al. Photonic topological insulators. *Nat. Mater.* **12**, 233 (2012).
38. Chen, W.-J. et al. Experimental realization of photonic topological insulator in a uniaxial metacrystal waveguide. *Nat. Commun.* **5**, 5782 (2014).
39. Wu, L.-H. & Hu, X. Scheme for achieving a topological photonic crystal by using dielectric material. *Phys. Rev. Lett.* **114**, 223901 (2015).
40. He, C. et al. Photonic topological insulator with broken time-reversal symmetry. *Proc. Natl Acad. Sci.* **113**, 4924–4928 (2016).
41. Ma, T. & Shvets, G. All-si valley-Hall photonic topological insulator. *N. J. Phys.* **18**, 025012 (2016).
42. Dong, J.-W., Chen, X.-D., Zhu, H., Wang, Y. & Zhang, X. Valley photonic crystals for control of spin and topology. *Nat. Mater.* **16**, 298–302 (2017).
43. Gao, F. et al. Topologically protected refraction of robust kink states in valley photonic crystals. *Nat. Phys.* **14**, 140–144 (2017).
44. He, X. T. et al. A silicon-on-insulator slab for topological valley transport. *Nat. Commun.* **10**, 872 (2019).
45. Shalaev, M. I., Walasik, W., Tsukernik, A., Xu, Y. & Litchinitser, N. M. Robust topologically protected transport in photonic crystals at telecommunication wavelengths. *Nat. Nanotechnol.* **14**, 31–34 (2019).
46. Lu, J., Qiu, C., Ke, M. & Liu, Z. Valley vortex states in sonic crystals. *Phys. Rev. Lett.* **116**, 093901 (2016).
47. Barik, S. et al. A topological quantum optics interface. *Science* **359**, 666–668 (2018).
48. Sun, X. C. et al. Ideal acoustic quantum spin Hall phase in a multi-topology platform. *Nat. Commun.* **14**, 952 (2023).
49. Chen, W. J., Zhang, Z. Q., Dong, J. W. & Chan, C. T. Symmetry-protected transport in a pseudospin-polarized waveguide. *Nat. Commun.* **6**, 8183 (2015).

50. Martini, E., Silveirinha, M. G. & Maci, S. Exact solution for the protected TEM edge mode in a PTD-symmetric parallel-plate waveguide. *IEEE Trans. Antennas Propag.* **67**, 1035–1044 (2019).

Author contributions

W.J.C. and J.W.D. conceived the project; F.L.S. and X.D.C. designed the samples; F.L.S. did the simulations and performed the experiments; F.L.S., X.D.C. and W.J.C. analyzed the data; F.L.S. and W.J.C. prepared the main manuscript with inputs from all authors; W.J.C. and J.W.D. supervised the project.

Competing interests

The authors declare no competing interests.

Additional information

Supplementary information The online version contains supplementary material available at https://doi.org/10.1038/s42005-024-01853-w.

Correspondence and requests for materials should be addressed to Wen-Jie Chen or Jian-Wen Dong.

Peer review information *Communications Physics* thanks Guanghui Ren and the other, anonymous, reviewer(s) for their contribution to the peer review of this work.

Reprints and permissions information is available at http://www.nature.com/reprints

Publisher's note Springer Nature remains neutral with regard to jurisdictional claims in published maps and institutional affiliations.